2019 International Symposium on Lightning Protection (XV SIPDA), São Paulo, Brazil, 30th September – 4th October 2019.

Electric Field of Horizontal Grounding Electrodes

Marco Aurélio O. Schroeder[a] Maria Teresa Correia de Barros[b] Antonio C. S. Lima[c] Rodolfo A. R. Moura[a]
Pedro Henrique Nascimento Vieira[a]

[a]Department of Electrical Engineering (DEPEL)
Federal University of São João del-Rei (UFSJ)
São João del-Rei, Brazil
schroeder@ufsj.edu.br, moura@ufsj.edu.br, pedrohnv@hotmail.com

[b]Instituto Superior Técnico (IST)
University of Lisbon (UL)
Lisboa, Portugal
teresa.correiadebarros@tecnico.ulisboa.pt

[c]Department of Electrical Engineering (DEE)
Federal University of Rio de Janeiro (UFRJ)
Rio de Janeiro, Brazil
acsl@dee.ufrj.br

***Abstract*—In this paper the electric field spatial distribution in the soil, generated by electric currents in horizontal electrodes, is calculated and analyzed. Two soil models are adopted; one considering constant electrical parameters and another that considers its variations with frequency. Two values of low-frequency soil resistivity are considered: one low (100 Ω.m) and one high (1000 Ω.m). Also are analyzed two electrode lengths, being one short (15 m) and the other long (60 m). The results illustrate that the electric field values show a large dependence on the soil model, the current source (transverse and longitudinal), the point of observation where the field is determined and the frequency.**

Keywords—Electric Field; Soil Model; Lightning; Frequency Domain.

I. INTRODUCTION

The lightning performance of electrical systems fundamentally depends on the grounding transient behavior [1,2]. The typical lightning current has a wide frequency spectrum, from a few Hz to tens of MHz [3]. Therefore, this current can generate induced voltages in electrical equipment located in the vicinity of the grounding electrodes.

In order to quantify the electromagnetic induction phenomenon, it is of the utmost importance to know the electric field at the soil surface generated by the currents that circulate in the grounding system [4,5].

It is also equally important to know the spatial distribution of the electric field inside the ground, in the vicinity of the electrodes. This knowledge can help, for example, the determination of maximum electric field levels on the electrode surface.

In addition, the calculation of the electric field inside the soil allows to establishing the depth in the soil where the electric field levels are still significant. From this last perspective, the electric fields inside the ground, generated by impulsive currents, calculated in the frequency domain, are presented in this paper. The frequency dependence of the electric field is investigated. Additionally, the influence of frequency dependence of the soil electrical conductivity and permittivity in the electric field values is also investigated considering models available in the literature.

The paper is organized into five sections. After this brief introduction, section 2 presents the background of calculation of electric field generated by lightning currents distributed in grounding electrodes. Section 3 presents the case studies used in this paper to obtain the results. In section 4 the results are described and in the 5 the respective conclusions are presented.

II. BACKGROUND: ELECTRIC FIELD CALCULATION

Initially, it is necessary to determine the distributions of electric currents along the electrode. This is accomplished by applying the HEM [6]-[8]. Then, the conservative (associated with the transverse currents) and non-conservative (associated to the longitudinal currents) components of the total electric field are calculated [9,10]. For determining the conservative component, the complex images method is used, according to [11]. For the non-conservative, the ideal image method is considered, according to [12].

The details of the two electric field component formulations can be verified in [9,10]. The mathematical expressions of the conservative and non-conservative components are as follows:

$$\vec{E}_{C_i} = \frac{1}{4\pi\left[\sigma(\omega)+j\omega\varepsilon(\omega)\right]} \int_{\ell_i} \frac{I_{Ti}}{\ell_i} \frac{(1+\gamma\, r_i)\, e^{-\gamma r_i}}{r_i^2} dl_i\, \hat{a}_{e_i} \quad (1)$$

$$\vec{E}_{NC_i} = -\,j\omega\, \frac{\mu_0}{4\pi} \int_{\ell_i} I_{Li} \frac{e^{-\gamma r_i}}{r_i} d\vec{l}_i \quad (2)$$

In Equations (1) and (2) we have the following quantities:

- $\vec{E}_{C_i}$ and $\vec{E}_{NC_i}$ are the conservative and non-conservative components of the total electric field, respectively, generated by the i-th segment of the electrode;
- I_{Ti} and I_{Li} correspond to the transverse and longitudinal currents of the i-th segment, respectively;
- r_i is the distance between the infinitesimal element dl_i and point P (generic point where the field is calculated);
- $\hat{a}_{e_i}$ is the unit vector that defines direction of $\vec{E}_{C_i}$;
- ℓ_i is the length of i-th segment;
- $d\vec{l}_i$ is the length vector element of i-th segment, which defines the direction of $\vec{E}_{NC_i}$;
- $\sigma(\omega)$, $\varepsilon(\omega)$ and μ_0 are the soil conductivity, permittivity and permeability, respectively (in general, for most cases, the magnetic permeability of the soil is close to that of the vacuum [13]);
- $\gamma = \sqrt{j\,\omega\,\mu[\sigma(\omega)+j\,\omega\,\varepsilon(\omega)]}$ is the propagation constant, being $\omega = 2\pi f$ the angular frequency.

As the studied system is considered linear, the total conservative and non-conservative components, as well as the total electric field, are calculated by summing all the contributions of the N segments that compose the electrode.

III. Case Studies

The "basic study case" corresponds to a horizontal electrode with length "L", radius "a" and buried at "d", whose geometric configuration is shown in Figure 1. The electric field is calculated along the "field observation line" indicated by FO in Figure 1. In this figure ρ_0 corresponds to the low-frequency soil resistivity and CI means "Current Injection" point.

The electrode shown in Figure 1 is immersed in a homogeneous, isotropic and linear soil. However, it is considered that soil can be dispersive. Thus, two soil models are considered:

- Constant soil parameters (ρ_0 and $\varepsilon_r = 15$);
- Frequency-dependent soil parameters according [14].

The following values are considered for the soil, electrode and lightning current quantities:

- Two values of ρ_0, being one soil with low (100 Ω.m) and another with high (1000 Ω.m) low-frequency resistivity;
- Two values of electrode length L, 15 m and 60 m, where a = 12 mm and d = 0.5 m are kept fixed;
- Four values of frequency, 100 Hz (low frequency), 50 kHz (low frequency), 200 kHz (first return stroke) e 1 MHz (subsequent return stroke).

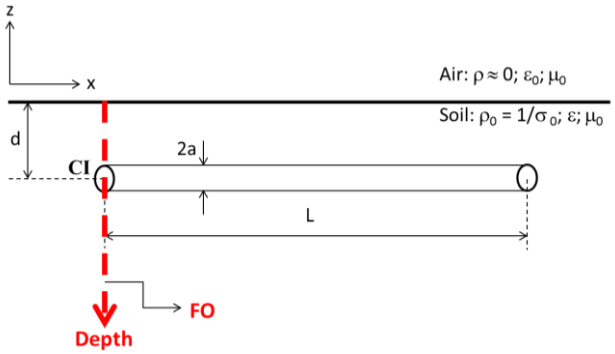

Figure 1 - Horizontal grounding electrode and field observation line (FO).

IV. Results and Discussions

Figure 2 shows the total electric field along FO (see Figure 1) considering L = 15 m and ρ_0 = 100 Ω.m for the frequencies of 100 Hz and 50 kHz. The left curves are associated with the constant soil parameter model, while the right curves are frequency-dependent soil parameters. Figure 3 is similar to Figure 2, considering however ρ_0 = 1000 Ω.m.

Figures 4 and 5 are similar to Figures 2 and 3, respectively, but with L = 60 m.

The frequencies considered in Figures 2 to 5 characterize phenomena of low-frequency (permanent regime and short circuit).

In order to analyze also transient phenomena, typical of lightning, Figures 6 to 9 show results similar to Figures 2 to 5, but with frequencies of 200 kHz (typical of the first return stroke currents) and 1 MHz (typical of subsequent return stroke currents).

The results presented in Figures 2 to 9 illustrate important physical aspects, among which the following are highlighted.

The soil model significantly influences the electric field levels. The electric field levels are reduced when considering the frequency-dependent soil parameters (when compared to the respective levels from the constant soil parameter model). This influence is more accentuated for soils with high resistivity values and for higher frequencies.

To illustrate in quantitative terms this influence, Table 1 shows the maximum electric field values of Figures 2 to 5, as well as the percentage reductions promoted by the frequency-dependent soil parameters. These percentages are calculated based on the maximum field value considering the constant soil parameters. Table 2 is similar, but for the cases of higher frequencies.

As can be seen in Table 1, the largest difference occurs at 1000 Ω.m and 50 kHz (23%), while in Table 2 it is close to 46% (1000 Ω.m and 1 MHz). However, significant differences are also found at 200 kHz to 1000 Ω.m (45%).

These influences are explained by the behavior of $\rho(f)$ and $\varepsilon_r(f)$ (frequency-dependence soil parameters) according to formulations proposed in [14]. Figure 10 illustrates $\rho(f)$ for the two values of ρ_0 considered in this paper, 100 Ω.m and 1000 Ω.m. The greatest variation is observed for ρ_0 higher and for the intermediate and higher frequencies. Figure 11 shows the behavior of $\varepsilon_r(f)$, where its decrease with frequency is observed. However, the term $\omega\varepsilon_r(f)\varepsilon_0$ increases with frequency. Of course, these variations directly impact the total electric field, according to Equations (1) and (2).

A very interesting fact refers to the influence of the increase of L.

In the case of low frequency (100 Hz) and low resistivity (ρ_0 = 100 Ω.m), when L increases from 15 to 60 m (Figures 2 and 4) there is a significant change (reduction) in electric field levels. This behavior is associated with the concept of low-frequency resistance that decreases with increasing electrode length. A similar situation also occurs for ρ_0 = 1000 Ω.m.

In the case of high frequencies (200 kHz and 1 MHz) and for ρ_0 = 100 Ω.m there are no differences in the electric field levels (see Figures 6 and 8), regardless of the value of L (15 or 60 m) and the soil model. This fact is associated to the effective electrode length, which in this case is close to 15 m. Thus, for lengths above 15 m there is no current flow through the electrodes.

For ρ_0 = 1000 Ω.m the situation is similar to that described above for frequency-dependent soil parameters (see right curves in Figures 7 and 9). Although L increases significantly (from 15 to 60 m) the frequency-dependence imposes a significant increase in soil conductivity, resulting in strong attenuations in the two frequencies, 200 kHz and 1 MHz. However, the situation is quite different in the case of constant soil parameters soil. With the increase of L from 15 to 60 m there is:

- Increase in electric field levels for f = 1 MHz and reduction of these levels to f = 200 kHz (see left curves in Figures 7 and 9).
- This behavior is associated with the vector compositions of the conservative and non-conservative components and with the propagation effect.

Another interesting aspect that can be verified on the basis of Figures 2 to 9 relates to the depth value in the soil from which the electric field is negligible.

To define this depth value it is necessary to define a metric. The authors analyzed this depth limit in a similar way to the concept of space constant applied in transmission lines, which defines the distance traveled by the wave so that its amplitude decreases to 37% of a previously established value. In the case of the application in this paper the value taken as base is the maximum electric field, which naturally occurs in z = - d (see Figure 1).

From the application of this methodology an unexpected result occurred: for all cases (Figures 2 to 9) the limit depth value was between -0.8 m and -0.9 m.

Table 1 - Maximum electric field values and the percentage reductions promoted by the frequency-dependent soil parameters referring to Figures 2 to 5.

L (m)	ρ_0 (Ωm)	Maximum electric field values (V/m) and percentage reductions (%)			
		Constant soil parameters		Frequency-dependent soil parameters	
		100 Hz	50 kHz	100 Hz	50 kHz
15	100	8.3	9.1	8.3 and 0%	8.6 and 5.5%
	1000	83.0	83.0	82.3 and 0.8%	64.0 and 23%
60	100	2.5	8.7	2.5 and 0%	8.5 and 2.3%
	1000	24.8	29.3	24.6 and 0.8%	22.6 and 23%

Table 2 - Maximum electric field values and the percentage reductions promoted by the frequency-dependent soil parameters referring to Figures 6 to 9.

L (m)	ρ_0 (Ωm)	Maximum electric field values (V/m) and percentage reductions (%)			
		Constant soil parameters		Frequency-dependent soil parameters	
		200 kHz	1 MHz	200 kHz	1 MHz
15	100	15	31	14 and 7%	27 and 13%
	1000	84	98	46 and 45%	61 and 38%
60	100	16	31	15 and 6%	27 and 13%
	1000	56	116	45 and 20%	63 and 46%

V. CONCLUSION

In this paper we present the preliminary results of the electric field spatial distribution in the soil, generated by electric currents in horizontal electrodes.

The initial results generally illustrate that:

- Models that neglect the component of the electric field due to longitudinal current in grounding electrodes, erroneously predict smaller electric field values.
- Distribution of the voltage and electric field along the conductor is not correctly predicted by such models.
- If the frequency dependence of soil electrical conductivity and permittivity is not included, the values of computed electric fields are overestimated, mainly for soils with high resistivity values and in the intermediate and higher frequency spectrum range.

VI. ACKNOWLEDGMENT

This study was financed in part by the Coordenação de Aperfeiçoamento de Pessoal de Nível Superior - Brasil (CAPES), Finance Code 001. It also was partially supported by INERGE (Instituto Nacional de Energia Elétrica), CNPq (Conselho Nacional de Desenvolvimento Científico e Tecnológico), FAPEMIG (Fundação de Amparo à Pesquisa do Estado de Minas), and FAPERJ (Fundação Carlos Chagas Filho de Amparo à Pesquisa do Estado do Rio de Janeiro).

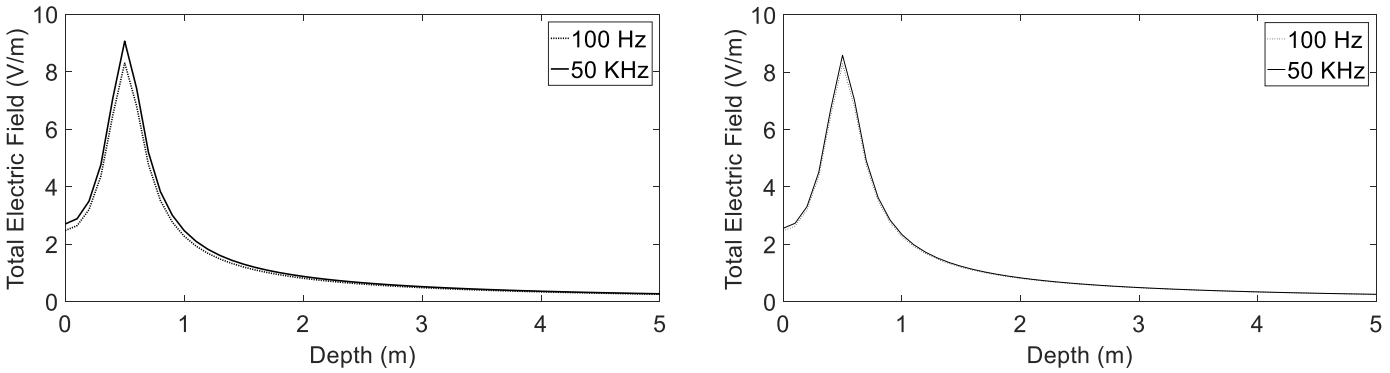

Figure 2 - Spatial distribution of the total electric field along FO (see Figure 1), considering L = 15 m and ρ_0 = 100 Ωm for frequencies of 100 Hz and 50 kHz. The left curves are associated with the with constant soil parameter model, while the right curves are frequency-dependent soil parameters.

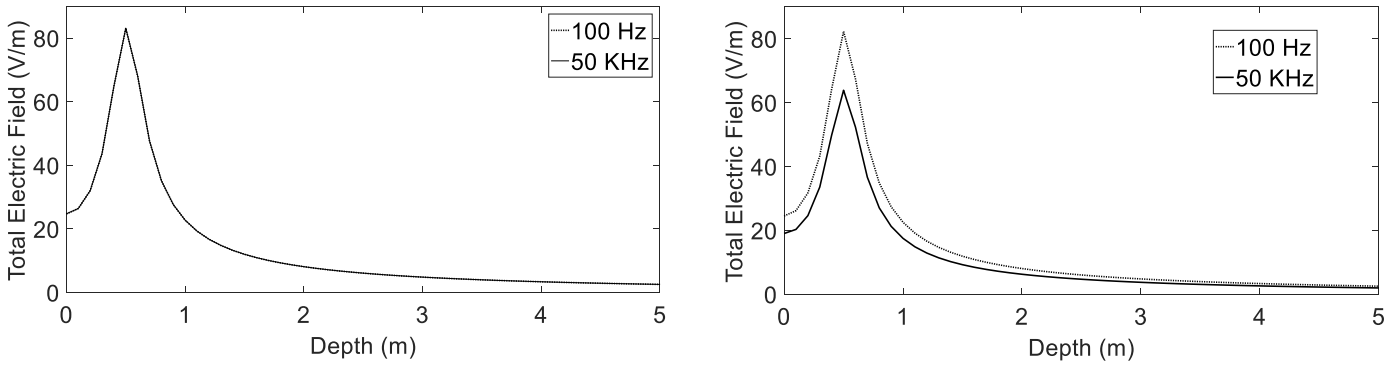

Figure 3 - Spatial distribution of the total electric field along FO (see Figure 1), considering L = 15 m and ρ_0 = 1000 Ωm for frequencies of 100 Hz and 50 kHz. The left curves are associated with the with constant soil parameter model, while the right curves are frequency-dependent soil parameters.

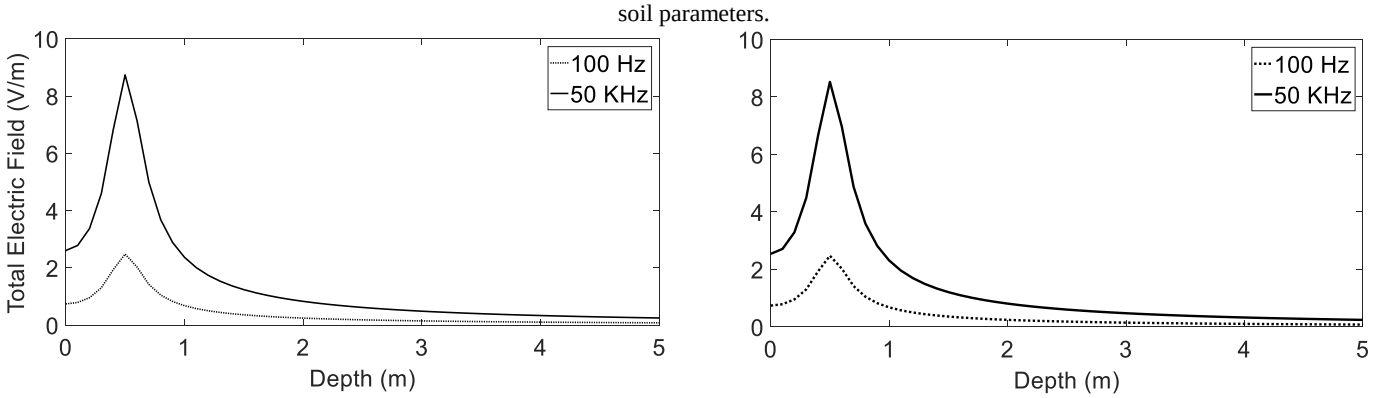

Figure 4 - Spatial distribution of the total electric field along FO (see Figure 1), considering L = 60 m and ρ_0 = 100 Ωm for frequencies of 100 Hz and 50 kHz. The left curves are associated with the with constant soil parameter model, while the right curves are frequency-dependent soil parameters.

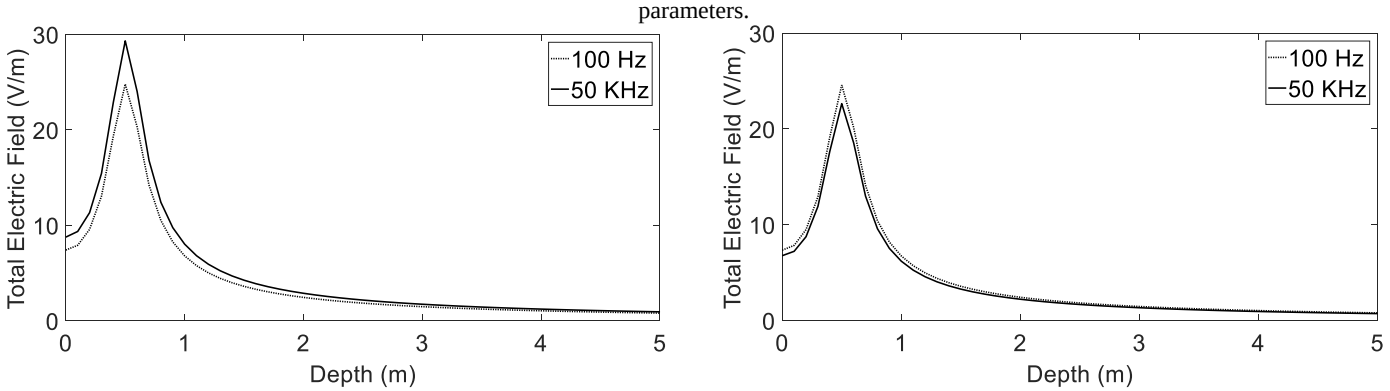

Figure 5 - Spatial distribution of the total electric field along FO (see Figure 1), considering L = 60 m and ρ_0 = 1000 Ωm for frequencies of 100 Hz and 50 kHz. The left curves are associated with the with constant soil parameter model, while the right curves are frequency-dependent soil parameters.

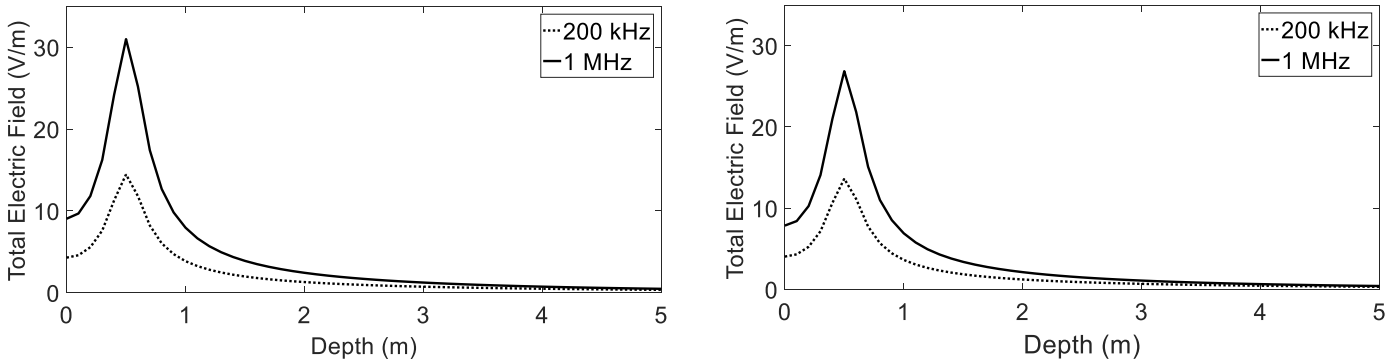

Figure 6 - Spatial distribution of the total electric field along FO (see Figure 1), considering L = 15 m and ρ_0 = 100 Ωm for frequencies of 200 kHz and 1 MHz. The left curves are associated with the with constant soil parameter model, while the right curves are frequency-dependent soil parameters.

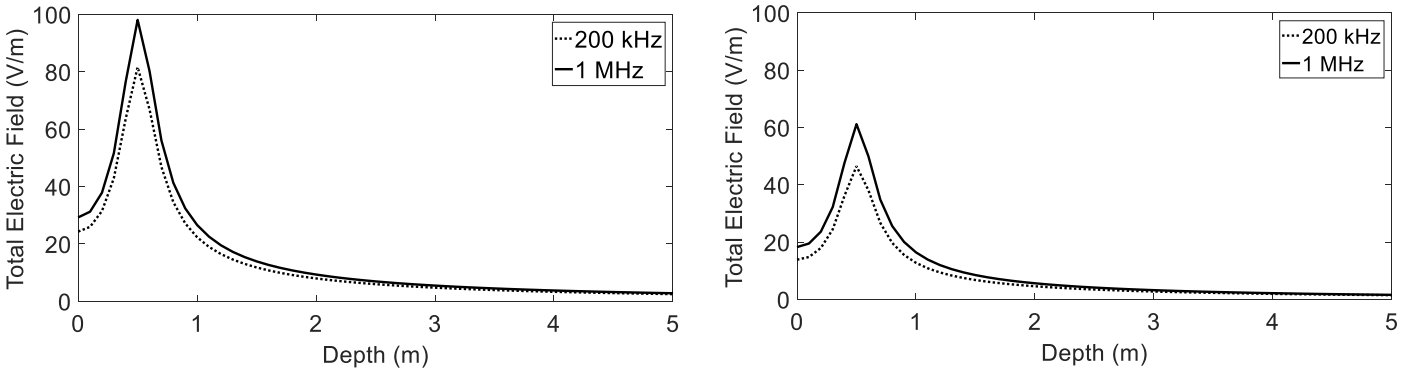

Figure 7 - Spatial distribution of the total electric field along FO (see Figure 1), considering L = 15 m and ρ_0 = 1000 Ωm for frequencies of 200 kHz and 1 MHz. The left curves are associated with the with constant soil parameter model, while the right curves are frequency-dependent soil parameters.

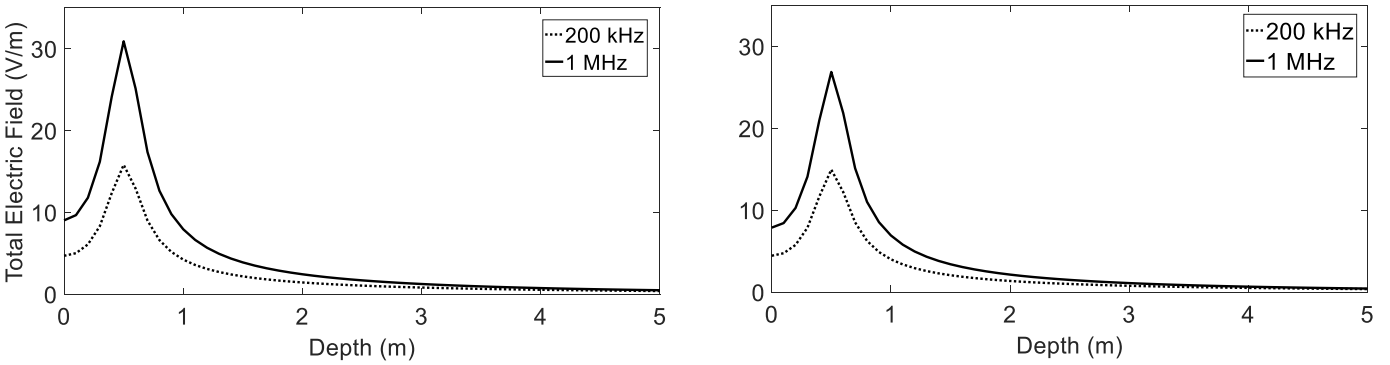

Figure 8 - Spatial distribution of the total electric field along FO (see Figure 1), considering L = 60 m and ρ_0 = 100 Ωm for frequencies of 200 kHz and 1 MHz. The left curves are associated with the with constant soil parameter model, while the right curves are frequency-dependent soil parameters.

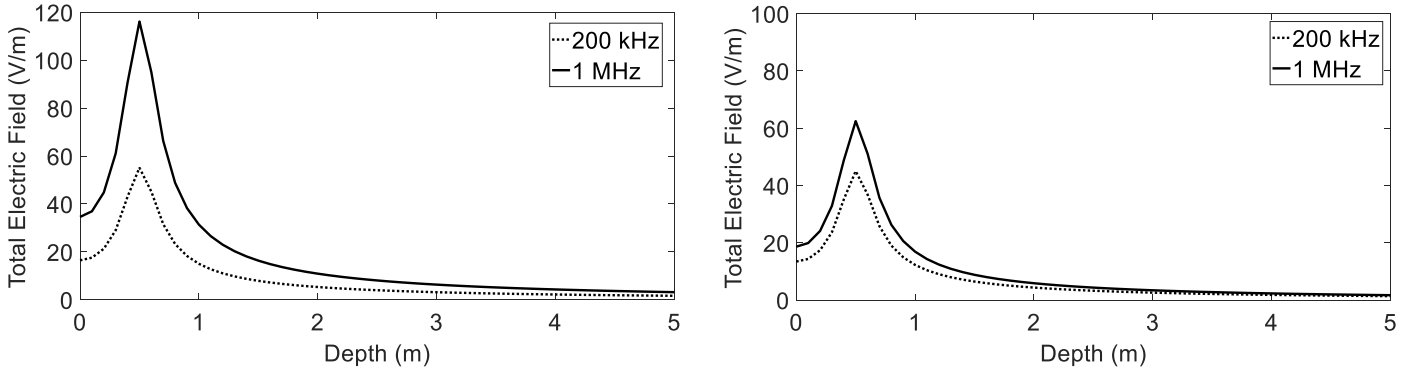

Figure 9 - Spatial distribution of the total electric field along FO (see Figure 1), considering L = 60 m and ρ_0 = 1000 Ωm for frequencies of 200 kHz and 1 MHz. The left curves are associated with the with constant soil parameter model, while the right curves are frequency-dependent soil parameters.

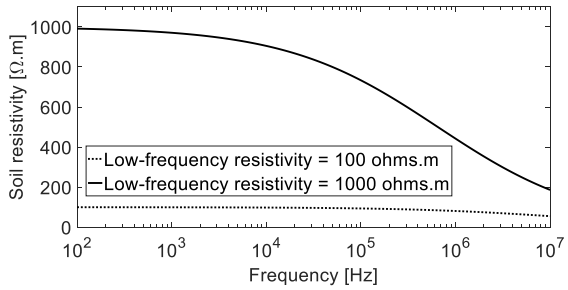

Figure 10 – Frequency-dependent soil resistivity according to [14] considering low-frequency soil resistivities: 100 Ω.m and 1000 Ω.m.

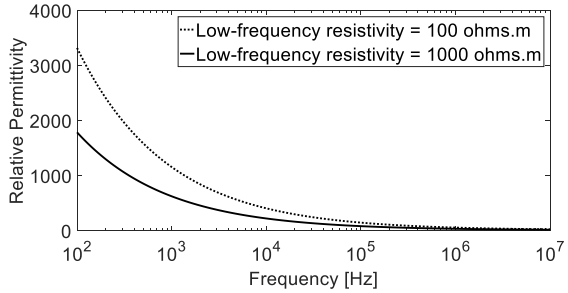

Figure 11 – Frequency-dependent soil permittivity according to [14] considering low-frequency soil resistivities: 100 Ω.m and 1000 Ω.m.

REFERENCES

[1] CIGRÉ WORKING GROUP C4.4.02. Protection of MV and LV Networks Against Lightning – Part 1: Common Topics. February 2006.

[2] CIGRÉ WORKING GROUP C4.4.02. Protection of MV and LV Networks Against Lightning – Part 2: Lightning Protection of Medium Voltage Networks. December 2010.

[3] Rakov, V., Uman, M. A. Lightning Physics and Effects, Cambridge Univ. Press, Jan. 8, 2007.

[4] Grcev, L. Computer analysis of transient voltages in large grounding systems. IEEE Trans. Power Del., vol.11, no. 2, pp. 815-823, Apr. 1996.

[5] Alipio, R., Schroeder, M. A. O., Afonso, M. M., Oliveira, T. A. S. and Assis, S. C. Electric Fields of Grounding Electrodes with Frequency Dependent Soil Parameters. Electric Power Systems Research (EPSR) 83, 220– 226, 2012.

[6] Visacro, S., Portela, C. Modelling of earthing systems for lightning protection applications, including propagation effects. Proc. Conference on Lightning Protection (ICLP), pp. 129-132 Berlim, September 1992.

[7] Visacro, S., Soares, A. and Schroeder, M.A.O. An Interactive Computational Code for Simulation of Transient Behavior of Electrical System Components for Lightning Currents. 26th International Conference on Lightning Protection (ICLP). 9b.3, Cracow, Poland, September 2-6, 2002.

[8] S. Visacro and A. Soares, "HEM: A model for simulation of lightning-related engineering problems", IEEE Trans. Power Delivery, Vol. 20, no. 2, pp. 1206-1207, 2005.

[9] Alípio, R.S., Schroeder, M.A.O., Afonso, M.M. and Oliveira, T A.S. Electromagnetic fields of buried conductors, Proc. Int. Conf. Grounding Earthing, pp. 399–402, 2008.

[10] Alípio, R.S., Schroeder, M.A.O., Afonso, M.M. and Oliveira, T A.S. Electric Fields of Grounding Electrodes: Frequency and Time Domain Analysis. X International Symposium on Lightning Protection, 9th-13th November, 2009 – Curitiba, Brazil.

[11] T. Takashima, T. Nakae, R. Ishibashi, Calculation of complex fields in conducting media, IEEE Trans. Electr. Insul. 15. February 1, 1980, pp. 1–7.

[12] Arnautovski-Toseva, V., Grcev, L. On the Image Model of a Buried Horizontal Wire. IEEE Transactions on Electromagnetic Compatibility, vol. 58, No. 1, pp. 278-286, February 2016.

[13] Portela, C. Frequency and Transient Behavior of Grounding Systems – I. Physical and Methodological Aspects. Proc. of the IEEE International Symposium on Electromagnetic Compatibility, Austin, U.S.A., pp. 379-384, 1997.

[14] Alipio, R. and Visacro, S. Modeling the frequency dependence of electrical parameters of soil. IEEE Transactions on Electromagnetic Compatibility, vol. 56, no. 5, pp. 1163–1171, Oct. 2014.